Hindawi
Advances in Materials Science and Engineering
Volume 2022, Article ID 9747505, 7 pages
https://doi.org/10.1155/2022/9747505

Research Article

Reactive Ion Etching (RIE) Induced Surface Roughness Precisely Monitored In-Situ and in Real Time by Reflectance Anisotropy Spectroscopy (RAS) in Combination with Principle Component Analysis (PCA)

Emerson Oliveira, Johannes Strassner, Christoph Doering, and Henning Fouckhardt

Integrated Optoelectronics and Microoptics Research Group, Physics Department, Technische Universität Kaiserslautern (TUK), P.O. Box 3049, Kaiserslautern D-67653, Germany

Correspondence should be addressed to Emerson Oliveira; candido@rhrk.uni-kl.de

Received 8 September 2022; Revised 9 October 2022; Accepted 1 November 2022; Published 11 November 2022

Academic Editor: Zhigang Zang

Reactive ion etching (RIE) of group IV or III/V semiconductors is an important step in many lithographic processes in semiconductor technology. Typically, surface roughness is undesired, but more and more applications arise where rough surfaces are used as functional quasi-layers. Either to avoid roughness or to precisely define it, in situ monitoring and control of the state of the etch front is desirable to increase yield. As we already know, reflectance anisotropy spectroscopy (RAS) or RAS equipment might be used to monitor the state of the etch front, to determine the current etch depth in situ precisely with accuracies of as good as some lattice constants only, and to identify roughness morphologies, the latter in combination with principle component analysis (PCA) and linear discriminant analysis (LDA). In cases where only one specific morphology with different characteristic parameters is under consideration, PCA suffices for monitoring, although the task is even harder. The PCA-RAS combination allows for distinguishing states of the etch front, which differ by a couple of minutes of etch duration only.

1. Introduction

Reflectance anisotropy spectroscopy (RAS) is a powerful in situ tool originally invented for precise monitoring of the state of the growth front during epitaxial processes [1–3]. MOCVD (metal-organic chemical vapor deposition) processes had been in mind, but RAS has been shown to work for MBE (molecular beam epitaxy) as well [4]. A lot of very valuable and interesting work has been done to understand the physical reasons for certain peaks in the RAS spectra. But for growth monitoring, the peaks' reproducibility is more important than their physical origin.

As in [5–7], RAS also works for the monitoring of the etch front in situ and in real time during reactive ion etching (RIE) processes, as long as the material desorption is not too chaotic, i.e., as long as the chemical etch component is not too strong. That means that desorption is not completely statistical; molecules preferably detach from the edges of existing surface clusters, similar but reversed to the adsorption of molecules at cluster edges during growth. Thus, the RAS spectra during growth and RIE are very similar.

The RAS equipment can also be used to determine the current etch depth with very high precision on the order of a couple of lattice constants [8, 9]. In this case, the Fabry-Perot oscillations of the genuine RAS signal spectra or of the average reflectivity spectra are used. These oscillations stem from the ever decreasing thickness of the uppermost (i.e., currently etched) semiconductor layer upon etching.

And recently, we have verified that RAS can even be employed to monitor surface roughness upon etching and to

identify different roughness morphologies with very high accuracy. This way, there is a chance to change etch parameters in real time either to avoid any roughness or to support a specific desired morphology in both cases, to increase yield.

This high accuracy of roughness morphology identification will be possible if RAS is combined with powerful statistical tools, namely, principle component analysis (PCA) and linear discriminant analysis (LDA) [10–12]. PCA is concerned with a principle axis transformation in cases with many "dimensions" and looks for the projection of the maximum data variance. We are dealing with up to 142 dimensions, i.e., the genuine RAS signals at 71 different photon energies and the average reflectivities at the same photon energies. In situations with many possible morphologies (due to a broad range of etch parameters), it is helpful to combine PCA with LDA. The latter is also a dimensionality reduction tool, but-as opposed to PCA-it is supervised, i.e., it uses prior "labeling" of categories, in our case labeling of different roughness morphologies, like "Wrinkles" or "Weak Ripples," to name just two examples. LDA finds the projection of the multidimensional space that results in the maximum separation between the known categories/labels. For situations with multiple possible morphologies, LDA alone is not sufficient because the method has problems with noisy signals. And PCA alone will not suffice if a reliable distinction between different morphologies is sought after.

But oftentimes, RIE processes deal with just a narrow range of etch parameters such that only a very specific surface morphology is to be expected. As we show in this contribution, in these cases, RAS can even be used to successfully identify certain parameter values of the evolving mesas and pillars (here their height). Then labeling is not necessary; the analysis does not need LDA, but just PCA and gets easier this way.

Throughout this contribution, we assume maskless RIE processes. But the method can also be applied to processes with etch mask as long as some unmasked area or window is provided for the RAS light spot of 4 mm diameter at the center of the wafer or sample [6].

Recent works with RIE point to applications such as surface modification for self-cleaning [13], antireflection [14], energy harvesting [15, 16], or metasurface fabrication [17, 18], for example. An opportunity to enhance such applications with in situ characterization might be possible with RAS monitoring.

2. RAS Principle

The genuine RAS signal is the difference ΔR in the optical reflectivity R of linearly polarized light at normal incidence between two perpendicular directions. Those are named x and y and are rotated 45 degrees with respect to the two main crystal axes, normalized by the mean reflectivity $\langle R \rangle$:

$$\frac{\Delta R}{\langle R \rangle}(h\nu) = \frac{R_x - R_y}{\left(R_x + R_y\right)/2}, \quad (1)$$

where the value depends on the photon energy $h\nu$ of the RAS light. Typical absolute values are around 10^{-3}.

In principle, for normal incidence, a plane of incidence as well as parallel or perpendicular light polarization should not be definable at all. But cluster edges on the growth, or, here, etch front break the symmetry and allow for the reflectivity difference [1, 19].

Typically, a spectrally broad light source, i.e., a Xe lamp, is used for RAS to be able to collect data for a broad range of photon energies (e.g., from 1.5 to 5.0 eV).

Oftentimes, the genuine RAS spectrum is used for evaluation, but sometimes the average reflectivity, i.e., the denominator in Equation (1), suffices or shows even more pronounced peaks in the spectrum.

We employed an EpiRAS system from Laytec, Berlin, Germany.

3. III/V Samples and Exemplary Roughness Morphology

For these investigations, we have prepared quite different samples, like GaSb and GaAs substrates or simple III/V layer systems on these substrates, and quite different morphologies depending on etch parameters and sample holder material (debris from the chamber walls and the holders changes the etch conditions). In Figure 1, four morphology examples are given, their SEM (scanning electron microscope) micrographs as well as their RAS spectrum after plasma switch-off. The upper two examples are from plain or simple GaSb wafer samples, and the other ones are from plain GaAs wafer samples.

Figure 1 reveals that different morphologies come with different RAS spectra, which makes morphology monitoring by RAS meaningful.

For reasons of clarity, in this contribution, we stick to just one sample type, i.e., fragments from original (not overgrown) undoped 2″ GaSb wafers from Wafer Technology, Milton Keynes, UK. We also remain with one particular—here exemplary—morphology, which we label "Brush Cut." The nomination becomes obvious from the SEM micrograph in Figure 2. And we rely on the 71 dimensions from the genuine RAS signal, according to Equation (1), in addition to the 71 dimensions from the average reflectivity.

The applied RIE parallel plate reactor is of type MicroSys 350 from Roth & Rau, Wuestenbrand, Germany.

Typical etch parameters to achieve the "Brush Cut" morphology on GaSb are as follows:

(i) A stainless steel clamp and sample holder

(ii) A gas pressure of $8.6 \cdot 10^{-3}$ hPa

(iii) A gas composition with 50 sccm of Ar and no Cl_2 (i.e., the etch process is nonreactive)

(iv) A microwave power of 57 W at 13.56 MHz

(v) A bias voltage of 700 V

We chose a morphology related to a nonreactive process as an example on purpose because, in this case, the etching is slow (etch rate $\approx 0.023\,\mu$m/min) and it becomes more

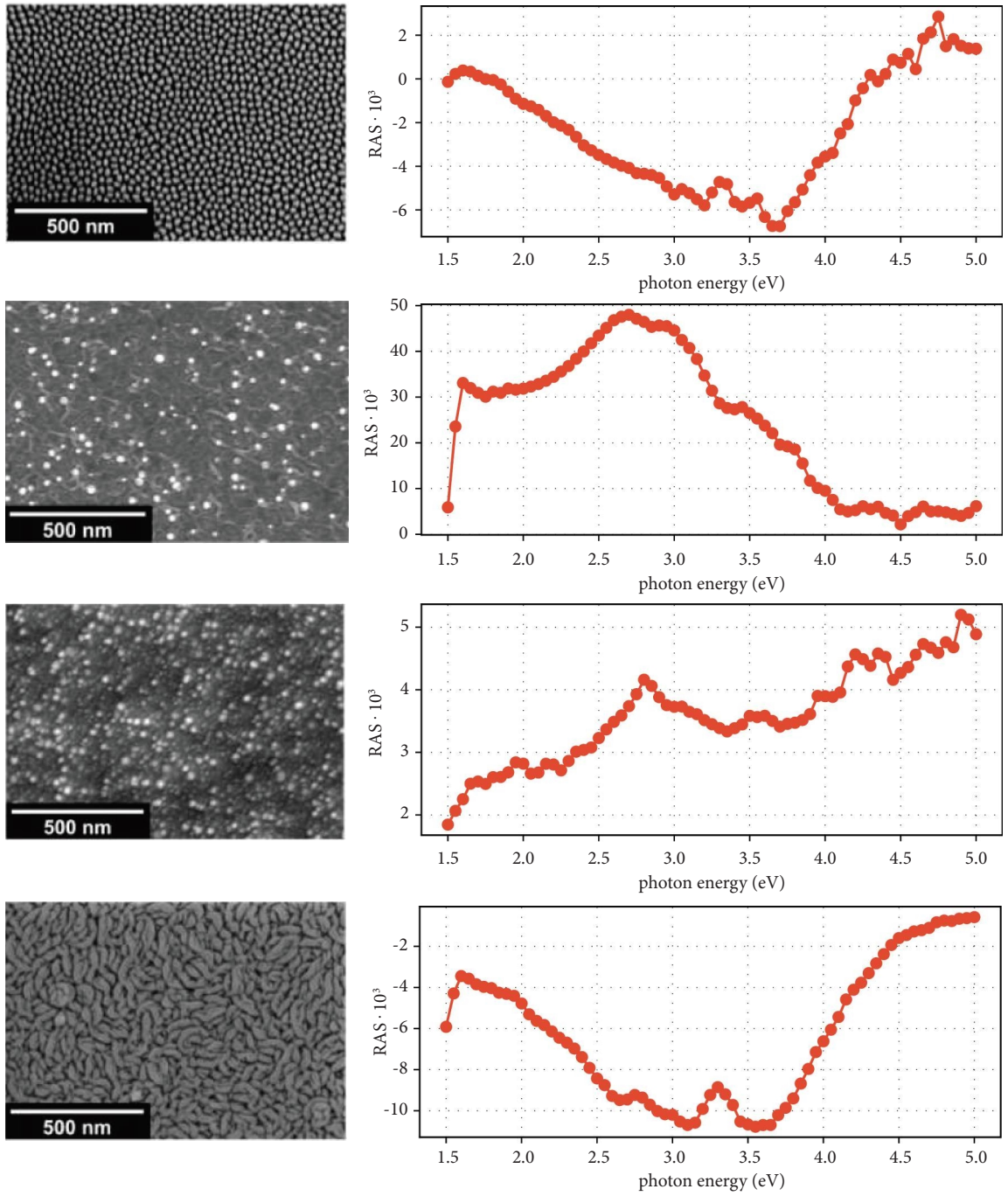

Figure 1: For four samples scanning electron microscope (SEM) images: (a) and related genuine RAS signal spectra. (b) The top two experimental results correspond to etching of plain GaSb wafers, the bottom ones to plain GaAs wafers.

obvious how small the surface changes might be, for which the genuine RAS signal is sensitive.

4. Principal Component Analysis (PCA)

PCA is used to reduce the dimensionality of a dataset in an interpretable way without losing much information [10, 11]. It allows for attributing specific scores to each genuine RAS data spectrum based on the variance of the set of samples. PCA is an unsupervised method, i.e., it does not need prior labeling of the samples and finds the linear combination, which represents the direction of maximum variance within the multidimensional data space. Maximum variance means the best possible distinction between data belonging to different samples. The application of PCA in the semiconductor industry is not new, see, e.g., [20, 21], but its combination with RAS during RIE is to the best of our knowledge.

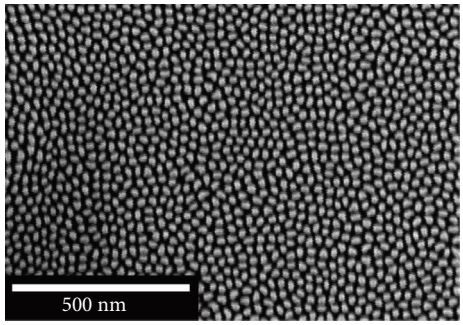

Figure 2: Scanning electron microscope (SEM) image of a "Brush Cut" morphology introduced during nonreactive ion etching (IE) of a GaSb wafer. Depending on etch time, the pillar (brush hair) height/width is quite different.

The analyzed data consist of the spectral data recorded after the etching process- "after" to begin with. If earlier data and PCA evaluations exist, the analysis can also be done in situ and in real time during the etch process and will give results, helpful to tune etch parameters "on the fly" as desired.

The data are subtracted by the respective spectra prior to etching and subsequently smoothed by the Savitzky-Golay algorithm [22]. For each sample, 71 genuine RAS signal values and 71 average reflectivity values are collected, each for a different photon energy (from 1.5 to 5.0 in 0.05 eV steps).

Any set of signals for each of the photon energies along the different samples will be called a feature. Thus, there are 71 features related to the genuine RAS signal spectra and 71 features related to the average reflectivity signal. Here, we employ four different samples with "Brush Cut" morphology.

To minimize the contribution of outliers in the dataset, a normalization algorithm is applied: the features are diminished by their respective averages and divided by their respective standard deviations. The number of the features is represented by the index i ($i = 1, \ldots, 71$) here, which spans the number of different photon energies, once for the genuine RAS signal and again for the average reflectivity. Thus, the feature signals are defined as follows:

$$\vec{Y}_i = \frac{\vec{y}_i - \overline{y}_i}{\sigma_i}, \tag{2}$$

$\vec{Y}_i$ is the normalized i^{th} feature vector, $\vec{y}_i$ is the unnormalized i^{th} feature vector, $\overline{y}_i$ the average within the i^{th} feature, and σ_i the standard deviation related to the i^{th} feature. After this normalization, the (dimensionless) features have a null average and a unit standard deviation. The initial standard deviations and averages stay recorded for later collection of data from additional samples for real-time evaluations.

The PCA algorithm calculates the covariance matrix, its eigenvectors, and its eigenvalues from the normalized data. The eigenvectors are sorted according to their eigenvalue in decreasing order, which can be interpreted as the contributions of each eigenvector to the total variance of the data. The scalar product of the eigenvector with the dataset for any one sample results in a score, being the value of the respective principal components, e.g., PC1, or PC2. By application of this mathematical procedure on different eigenvectors, the desired number of principal components (PCs) is obtained [11]. The whole procedure is identical to making a principle axis transformation, e.g., in mechanics, for the rotation of the ellipsoid of the moments of inertia in three dimensions. But in this contribution, we deal with many more dimensions, i.e., either 71 or 142, as mentioned above.

In principle, any user of the RIE-RAS-PCA combination, which is newly reported here, should be aware that the PCs are not necessarily directly related (not to speak of proportional) to specific pillar parameters. The optical reflectivity from which the PCs are deduced depends on many parameters, like pillar height, width, distance, aspect ratio, and maybe more. Their influences might be interrelated in a complicated manner. Even then, e.g., a plot of the first principal component for the genuine RAS signal versus the first principal component for the average reflectivity signal might give distinct spots for different etch fronts of the same morphology. This might already be helpful for RIE monitoring and etch front characterization. But in our exemplary case, fortunately, PC1 for RAS is nearly proportional to etch time, and PC1 for average reflectivity is nearly proportional to the height of the pillar or brush hair, as will also be demonstrated below.

5. Results

Figure 3 presents the final genuine RAS spectra for the samples of "Brush Cut" morphology with different etch times. Samples are labeled A (1 min etching), B (5 min), C (10 min), and D (35 min) and are color coded. The spectra presented in Figure 3 are subtracted from their respective spectra prior to etching and fed into the PCA algorithm. Figure 4 gives the resulting first principal components of PC1 for genuine RAS ($PC1_{RAS}$) and for the average reflectivity ($PC1_{\text{average reflectivity}}$) for such samples. The same etch parameters have been applied for the experiments as mentioned in Section 3.

The PCA evaluation has been done after the completion of all four etch processes. But considering the retrieved eigenvectors and the stored RAS and reflectivity spectra, it would also be possible to identify specific spots in the chart, which relate to the samples and their intermediate RAS and reflectivity spectra at specific points in time before the end of the etch process. Those spots are marked partially transparent and make a visualization of the surface state evolution over the current etch time possible. For example, sample B with 5 min of overall etch duration evolves from the situation and chart spot after 1 min of etching which is identical to the situation and chart spot for sample A with 1 min overall etch duration into the situation and spot after 5 min.

It is obvious from the PC chart in Figure 4 that even slight changes in etch time result in different spot positions in the chart, which reveals the sensitivity of the technique. Considering the fact that we use a morphology example here,

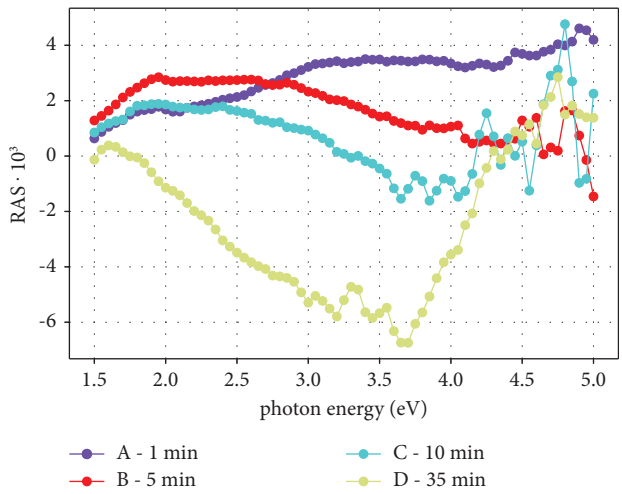

Figure 3: RAS spectra for samples A, B, C and D lines are just guide to the eyes.

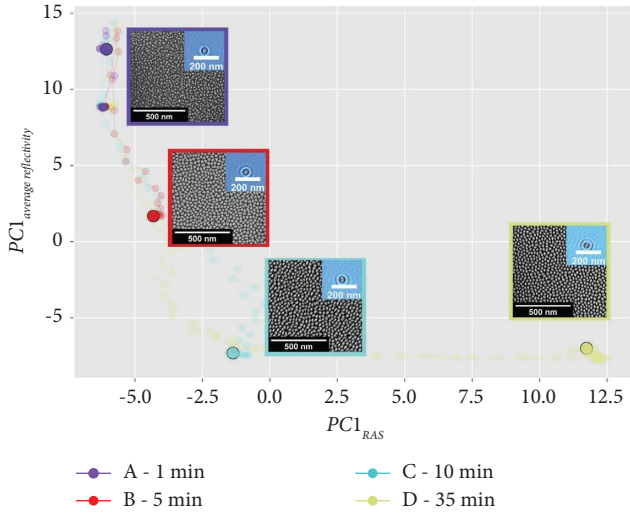

Figure 4: $PC1_{RAS}$ and $PC1_{\text{average reflectivity}}$ evolutions and scanning electron microscope (SEM) images of "Brush Cut" morphologies introduced during reactive ion etching (RIE) of GaSb substrates. Insets in the SEM micrographs correspond to their two-dimensional spatial autocorrelations.

which is related to a nonreactive and, thus, slow ion etch process, this sensitivity also applies to minor changes in the surface roughness.

Figure 4 also reveals that $PC1_{RAS}$ monotonically increases with etch time while $PC1_{\text{average reflectivity}}$ decreases. As the etch time progresses, so does the morphology development, increasing the RAS signal due to the emerging and increasing anisotropies caused by the roughness formation. On the other hand, the average reflectivity (i.e., the zeroth order scattering) decreases as scattering is more likely on a rough surface. So, it is worthwhile to investigate whether a pillar parameter follows the behavior of the PCs with etch time.

To retrieve the characteristic parameters of samples A through D, we cleaved the samples into two parts and inspected their cross sections with an SEM again. One of those SEM micrographs, i.e., the one for sample D, is exemplarily given in Figure 5.

Table 1 lists the important pillar parameters of the four samples which have been collected by the SEM sample inspection and the two-dimensional spatial autocorrelations from such images. From the autocorrelations, it can be seen that the pillars are, in general, elliptical.

Indeed, the pillar height inversely follows the evolution of the first principal component for the average reflectivity. Of course, reflectivity must be closely related to the height and width of the reflecting/scattering entities.

Figures 6 and 7 show plots of the dependencies of $PC1_{RAS}$ on etch time and $PC1_{\text{average reflectivity}}$ on pillar height, respectively.

This finding reveals that RAS, together with PCA analysis, allows for retrieving the pillar height with high accuracy. Of course, for in situ analysis, a set of formerly evaluated samples has to exist, from which the PC chart is calculated and the pillar heights can be calibrated to extract them in situ and in real time.

Nevertheless, it has to be stressed that the different principal components (PC1 to PCx), retrieved from the statistical PCA analysis, are not necessarily and in general will not be proportional, inversely proportional, or otherwise directly related to one specific characteristic pillar parameter. This dependence is highly related to the type of data being analyzed with the PCA and can vary enormously. A principle component might be proportional to the difference in the squares of two physical parameters, just to name one example (also taken from mechanics and the theory of moments of inertia).

In the context of RAS or reflectivity data evaluation, we also expected a complicated dependence of the principle components on pillar data because the PCs are statistically retrieved from reflectivity values in a complicated manner, and the reflectivity itself is dependent on different parameters of the received etch front. But in our case, obviously, there are some simple interdependencies, as mentioned above.

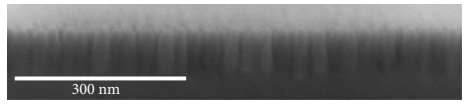

Figure 5: Scanning electron microscope (SEM) image of the cross section of "Brush Cut" morphology for sample D.

Table 1: List of characteristic pillar/brush hair parameters for the four samples of "Brush Cut" morphology.

Sample	Etch time (min)	Height (nm)	Width (nm)	Aspect ratio	Average pillar distance (nm)
A	1	21	30.1	0.79	18.7
B	5	61	28.1	2.42	16.4
C	10	70	36.2	2.40	17.6
D	35	80	31.1	3.13	15.4

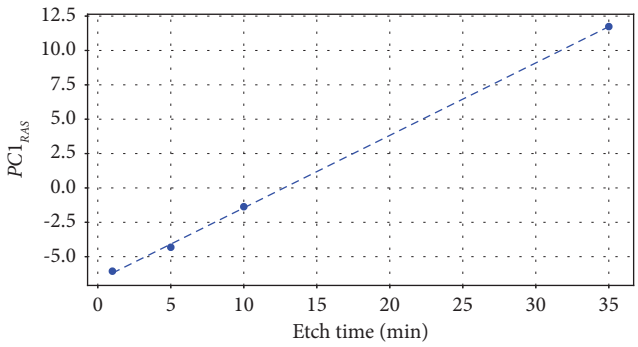

Figure 6: Dependence of $PC1_{RAS}$ on etch time: both quantities are nearly proportional.

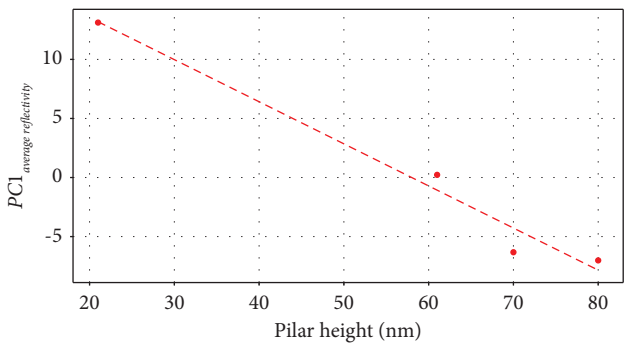

Figure 7: Dependence of $PC1_{average\ reflectivity}$ on pillar height: both quantities are inversely proportional in first approximation.

But even in cases where there is no direct (and thus simple) relation between some specific PCs and specific "pillar" parameters, the principle component analysis (PCA) and the calculated PC chart will be helpful because distinct spots in the chart will apply to distinct etch times. Thus, the combination of RIE-RAS and PCA is even helpful to distinguish etch fronts within the same class of roughness morphology.

6. Conclusions

Over the last 35 years, reflectance anisotropy spectroscopy (RAS) has proved to be a powerful method for monitoring and subsequent in situ control of epitaxial growth fronts as well as etch fronts in group IV and III/V semiconductor technology. This contribution is emphasizing the use of RAS during (maybe reactive) ion etching (RIE).

Earlier work has shown that RAS can be used during RIE for precise in situ determination of the current etch depth. Moreover, it has been verified by us that RAS (to be published elsewhere) combined with powerful statistical tools can be employed for the identification of different surface roughness morphologies with high accuracy.

In this contribution, we have shown that this latter finding can be extended to an extreme situation, i.e., for different samples of the very same surface roughness morphology.

Using principle component analysis (PCA) as the statistical tool, surfaces of different samples can be distinguished, which differ by minor changes in etch time and surface parameters only.

In our example, the physical quantity, which influences the average reflectivity data and its first principle component (PC1) most, is the height of the etched pillars/mesas. But even in cases where there was no simple relationship between a specific principle component and a specific pillar parameter, PCA would be helpful because distinct spots in a chart of two relevant principle components (e.g., in a PC plot) would apply to distinct etch times and etch fronts.

With a stored set of RAS spectra from earlier similar samples, the reported method can even be applied for new etch processes in situ and in real time with the help of intermediate RAS spectra.

The newly introduced RIE-RAS-PCA combination gives another degree of freedom to in situ monitoring and control of RIE processes and will increase the yield considerably.

Data Availability

Data that support the findings of this study are available from the corresponding author upon reasonable request.

Conflicts of Interest

The authors declare that there are no conflicts of interest regarding the publication of this paper.

Acknowledgments

This research has been funded by the German Research Foundation (Deutsche Forschungsgemeinschaft, DFG) under contracts FO 157/63-1 and FO 157/58-1. The authors are thankful for the above-mentioned funding. The research group is a member of the users' group of the Nano Structuring Center (NSC) of the Technische Universität Kaiserslautern (TUK) and is thankful for general NSC assistance. The authors would also like to thank Guilherme Sombrio for his early work on this subject.

References

[1] D. E. Aspnes, J. P. Harbison, A. A. Studna, and L. T. Florez, "Application of reflectance difference spectroscopy to molecular-beam epitaxy growth of GaAs and AlAs," *Journal of Vacuum Science and Technology A*, vol. 6, no. 3, pp. 1327–1332, 1988.

[2] J. T. Zettler, K. Haberland, M. Zorn et al., "Real-time monitoring of MOVPE device growth by reflectance anisotropy spectroscopy and related optical techniques," *Journal of Crystal Growth*, vol. 195, no. 1-4, pp. 151–162, 1998.

[3] P. Weightman, D. S. Martin, R. J. Cole, and T. Farrell, "Reflection anisotropy spectroscopy," *Reports on Progress in Physics*, vol. 68, no. 6, pp. 1251–1341, 2005.

[4] D. Hoffman, T. Loeber, and H. Fouckhardt, "In-situ Reflectance Anisotropy Spectroscopy (RAS) for doping control during MBE growth of AlGaInAsSb laser structures," in *Proceedings of the in 16th European Molecular Beam Epitaxy Workshop, Poster No. MoP11*, Alpe d'Huez, France, 2011.

[5] L. Barzen, J. Richter, H. Fouckhardt, M. Wahl, and M. Kopnarski, "Monitoring of (reactive) ion etching (RIE) with reflectance anisotropy spectroscopy (RAS) equipment," *Applied Surface Science*, vol. 328, pp. 120–124, 2015.

[6] A. K. Kleinschmidt, L. Barzen, J. Strassner et al., "Precise in situ etch depth control of multilayered III-V semiconductor samples with reflectance anisotropy spectroscopy (RAS) equipment," *Beilstein Journal of Nanotechnology*, vol. 7, pp. 1783–1793, 2016.

[7] L. Barzen, A. K. Kleinschmidt, J. Strassner et al., "Influence of plasma composition on reflectance anisotropy spectra for in situ III-V semiconductor dry-etch monitoring," *Applied Surface Science*, vol. 357, pp. 530–538, 2015.

[8] G. Sombrio, E. Oliveira, J. Strassner, J. Richter, C. Doering, and H. Fouckhardt, "Doped or quantum-dot layers as in situ etch-stop indicators for III/V semiconductor reactive ion etching (RIE) using reflectance anisotropy spectroscopy (RAS)," *Micromachines*, vol. 12, no. 5, p. 502, 2021.

[9] G. Sombrio, E. Oliveira, J. Strassner, C. Doering, and H. Fouckhardt, "Interferometric in-situ III/V semiconductor dry-etch depth-control with ±0.8 nm best accuracy using a quadruple-Vernier-scale measurement," *Journal of Vacuum Science & Technology B*, vol. 39, no. 5, Article ID 052204, 2021.

[10] H. Hotelling, "Analysis of a complex of statistical variables into principal components," *Journal of Educational Psychology*, vol. 24, no. 6, pp. 417–441, 1933.

[11] I. Jolliffe, "Principal component analysis," in *International Encyclopedia of Statistical Science*Springer Berlin Heidelberg, Berlin, Germany, 2011.

[12] R. A. Fisher, "The use of multiple measurements in taxonomic problems," *Annals of Eugenics*, vol. 7, no. 2, pp. 179–188, 1936.

[13] Y. Wu, Y. Wang, W. Yang et al., "Self-cleaning titanium dioxide metasurfaces with UV irradiation," *Laser & Photonics Reviews*, vol. 15, no. 2, Article ID 2000330, 2021.

[14] A. A. Bushunov, M. K. Tarabrin, and V. A. Lazarev, "Review of surface modification technologies for mid-infrared antireflection microstructures fabrication," *Laser & Photonics Reviews*, vol. 15, no. 5, Article ID 2000202, 2021.

[15] Z. Zang, "Efficiency enhancement of ZnO/Cu2O solar cells with well oriented and micrometer grain sized Cu2O films," *Applied Physics Letters*, vol. 112, no. 4, Article ID 042106, 2018.

[16] L. Wang, Y. Song, W. Xu et al., "Harvesting energy from high-frequency impinging water droplets by a droplet-based electricity generator," *EcoMat*, vol. 3, no. 4, pp. 1–9, 2021.

[17] B. Liu, Q. Zhang, L. Li et al., "Close-packed storage of potassium metallic clusters achieved through nanostructure engineering of ultrafine hollow nanoparticles-based carbon nanoclusters," *EcoMat*, vol. 3, pp. 1–11, 2021.

[18] F. Yue, R. Piccoli, M. Y. Shalaginov et al., "Nonlinear mid-infrared metasurface based on a phase-change material," *Laser & Photonics Reviews*, vol. 15, no. 3, Article ID 2000373, 2021.

[19] D. E. Aspnes and A. A. Studna, "Anisotropies in the above-band-gap optical spectra of cubic semiconductors," *Physical Review Letters*, vol. 54, no. 17, pp. 1956–1959, 1985.

[20] R. Shadmehr, D. Angell, P. B. Chou, G. S. Oehrlein, and R. S. Jaffe, "Principal component analysis of optical emission spectroscopy and mass spectrometry: application to reactive ion etch process parameter estimation using neural networks," *Journal of the Electrochemical Society*, vol. 139, no. 3, pp. 907–914, 1992.

[21] J. Yu and X. Lu, "Wafer map defect detection and recognition using joint local and nonlocal linear discriminant analysis," *IEEE Transactions on Semiconductor Manufacturing*, vol. 29, no. 1, pp. 33–43, 2016.

[22] A. Savitzky, M. J. E. Golay, and S. Golay, "Smoothing and differentiation of data by simplified least squares procedures," *Analytical Chemistry*, vol. 36, no. 8, pp. 1627–1639, 1964.